HAL
open science

Temperature dependence of the electrochemical behavior of the 690 Ni-base alloy between 25 and 325 °C

Salma El Euch, Damien Bricault, Hubert Cachet, Eliane Sutter, Mai T T Tran, Vincent Vivier, Nathalie Engler, Antoine Marion, Milan Skocic, Benjamin Huerta-Ortega

To cite this version:

Salma El Euch, Damien Bricault, Hubert Cachet, Eliane Sutter, Mai T T Tran, et al.. Temperature dependence of the electrochemical behavior of the 690 Ni-base alloy between 25 and 325 °C. Electrochimica Acta, 2019, 317, pp.509-520. 10.1016/j.electacta.2019.05.131 . hal-02164590

HAL Id: hal-02164590

https://hal.science/hal-02164590v1

Submitted on 25 Jun 2019

HAL is a multi-disciplinary open access archive for the deposit and dissemination of scientific research documents, whether they are published or not. The documents may come from teaching and research institutions in France or abroad, or from public or private research centers.

L'archive ouverte pluridisciplinaire **HAL**, est destinée au dépôt et à la diffusion de documents scientifiques de niveau recherche, publiés ou non, émanant des établissements d'enseignement et de recherche français ou étrangers, des laboratoires publics ou privés.

Temperature dependence of the electrochemical behavior of the 690 Ni-base Alloy between 25 and 325°C

Salma EL EUCH[1,2], Damien BRICAULT[1], Hubert CACHET,[1] Eliane M.M. SUTTER[1], Mai T.T. TRAN[1], Vincent VIVIER[1], Nathalie ENGLER[2], Antoine MARION[2], Milan SKOCIC[3], Benjamin HUERTA-ORTEGA[3]

(1) Sorbonne Université, CNRS, Laboratoire Interfaces et Systèmes Electrochimiques, LISE, F-75005 Paris, France

(2) Framatome, La Défense Paris, France

(3) Framatome Centre Technique, Le Creusot, France

Abstract

The electrochemical behavior and the chemical composition of passive films formed on the Alloy 690 at room temperature in borate buffer solution (pH = 9.0) was studied with different techniques for two surface finishings. XPS and quantum yield measurements showed the presence of Ni and Cr oxides and hydroxides for passive films formed on both the as received and the mechanically polished one, whereas the presence of mixed spinel type $Ni_{(1-x)}Fe_xCr_2O_4$ was only observed on the as received material. Additionally, Electrochemical Impedance Spectroscopy (EIS) highlighted a higher corrosion resistance for the as received alloy in comparison with the mechanically polished alloy, which was linked to the chemical composition of the oxide film. Electrochemical measurements were performed before, during, and after oxidation of the Alloy 690 of Steam Generator (SG) tube of Pressurized Water Reactor (PWR) at high temperature and high pressure in the simulated primary circuit of PWR. At high temperature, the interface becomes electrochemically active yielding the precipitation of the corrosion products which form a few tens of nm thick diffusion barrier for the released metal cations. This overlayer is built on the top of a few nm thick, Cr rich inner layer at the alloy/oxide interface which was found to behave similarly to that initially formed at ambient temperature. It is concluded that high temperature oxidation in the static condition of an autoclave at 325°C does not promote a better passivation state than the one already existing initially.

Keywords

Ni-base alloys; Oxide film; Electrochemical Impedance Spectroscopy; Photoelectrochemistry; XPS

1. Introduction

Nickel-base Alloys and in particular the Alloy 690 are the main manufacturing material for steam generator (SG) tubes of pressurized water reactors (PWRs) due to their high corrosion resistance, in particular to stress corrosion cracking. However, general corrosion of Ni-base alloys occurs in high temperature water leading to the contamination of the PWR primary circuit with the ^{58}Co radionuclide. ^{58}Co originates from the activation of Ni in the core of the reactor after being released from SG tubes. The oxide film formed on the Ni-base alloys has a key role in Ni release, as well as the PWR environment and the material characteristics that can also influence the passive film growth [1] [2].

The electrochemical and the oxide film properties have been extensively studied in order to understand the mechanism of Ni release from Ni-base Alloys and elucidate the growth mechanism of the oxide film at high temperature and high pressure [3] [4] [5]. The oxide film formed within the PWR media is generally described as a duplex oxide layer with an inner layer enriched in Cr and an outer layer that contains mainly nickel ferrite and nickel hydroxide [5] [6]. The internal part of the oxide film results from anionic diffusion through grain boundaries and local dislocations of the material surface [2] [7] generating an internal layer rich in Cr_2O_3. The external part of the film generally results from precipitation, due to local saturation of the media, of Ni and Fe ions after being released from the alloy forming nickel ferrite crystallites [6].

Hence, the Cr-rich layer within the passive film is considered to be the main factor of corrosion resistance of these alloys [8]. Additionally, semiconducting properties are also observed for the passive film formed on the Alloy 690 at high temperature, in agreement with the presence of rich Cr (n type semiconductor). However, there is no straightforward link between semiconducting properties, which are governed by the electron conduction, and corrosion resistance which is mostly governed by oxide stability and ion migration. Hur et al. [9] reported that mainly a n-type semi-conductive behavior was observed for the passive film formed on the Alloy 690 at high temperature. Interestingly, they also linked this result with the higher Cr content within the passive film. However, it was also reported that the oxide film growth and the Ni release depend on the sub-surface defects density of the material. Jeuland et al. [2] showed a correlation between the defect concentration and the oxygen diffusion in the oxide film. Moreover, the cold working of the surface state has an influence on the properties of the passive film, and consequently on the corrosion resistance of the alloy [10] [11]. The native film formed on Ni base alloy is described as an amorphous oxide layer with a duplex structure having an inner part mainly formed of Cr_2O_3 and mixed Ni and Cr hydroxides for the external part of the film [12]. Some authors mention the presence of a minor percentage of Fe within this native film [13]. At room temperature, the mechanism governing the formation of the passive film is based on the oxygen affinity of the alloy's elements (Cr>Fe>Ni) that migrate and form the oxide film at the material surface [14].

Most of the existing works on the Alloy 690 are performed at high temperature and high pressure [5] [2] [6], and only few studies have focused on the chemical composition and the electronic structure of the passive film formed on the surface of these alloys at room temperature [14] [15]. On the other hand, some authors suggest that Ni-base alloy behavior regarding the Ni-release strongly depends on the first stage of oxidation [16]. Although the chemical composition and electronic structure of the passive film formed on Ni base alloy are extensively studied at high temperature, the relationship between the film structure and its corrosion resistance properties still need to be investigated. Therefore, we assume that the structure and the composition of the native passive film formed on Alloy 690 govern the growth mechanism of the oxide layer on Ni-base alloy when exposed to PWR environment. More specifically, the structural defects already existing within the native passive

film (thus formed at low temperature) may control the protective properties of the oxide film further formed at high temperature.

The main objective of this work is to make a link between the native oxide film formed on Alloy 690 and the corrosion resistance of the material when it is used at higher temperature, which thus require the study of the passive film formed at high temperature within PWR primary water. The investigation at room temperature is thus required since it allows to obtain the characterization on the native passive film at the Alloy/oxide which becomes the starting inner passive layer under high temperature oxidation. In the following, it will be demonstrated that the inner layer formed at 325°C within static autoclave conditions exhibits similarities with the native passive film.

This work investigates the composition and the electrochemical response of passive film formed on the Alloy 690 at room and high temperature on the basis of electrochemical impedance spectroscopy. Photoelectrochemical measurements and surface analyses were also performed in order to better describe the general corrosion behavior of Ni-base alloys.

2. Experimental procedure

Industrial steam generator (SG) tubes of Alloy 690 were used as sample material in this study. Samples were machined from SG tubes to obtain a straight section of a quarter of the SG tube of 1.09 mm thickness and 19 mm outer diameter. Two different surface states of Alloy 690, mechanically polished (MP) and as received (AR) made by cold-rolling, were studied in this work. Figure 1 shows SEM observations of the both surface shapes before any electrochemical experiment. Moreover, the samples were analyzed by XPS before electrochemical measurements. The XPS spectra highlighted the presence of Ni and Cr oxides and hydroxides with the presence of the peaks related to the metallic compounds which suggest the existence of a thin film on the alloy surface.

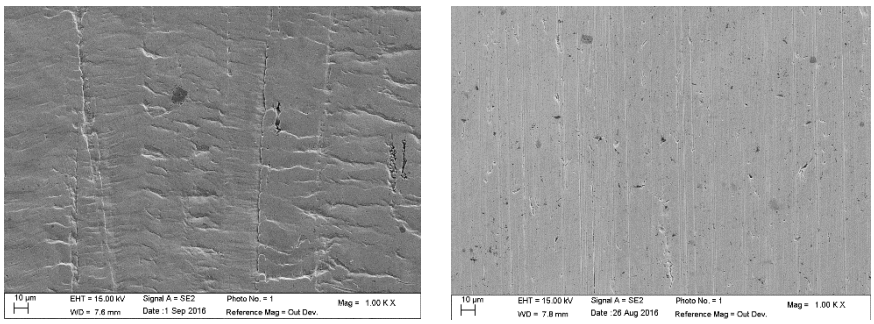

AR **MP**

Figure 1: SEM images of the surface state shape of the AR and MP samples

The general chemical composition of the alloy used in this work is reported in Table 1.

Table 1: Chemical composition of Alloy 690 (wt.%)

Material	Ni	Cr	Fe	Al	Ti	Si	P	Mn	C	S
Alloy 690	59	29	10.5	-	0.5	≤0.5	≤0.01	≤0.5	0.02	≤0.015

The mechanically polished tube was grinded using SiC papers down to grade 1200, then it was degreased and cleaned in ultrasonic bathes of successively ethanol and distilled water. The as received tubes were simply cleaned and degreased before analysis. The samples were mounted as working electrodes and their outer surface, as well as the cut borders, were covered by a commercial insulating

paint (Masking Aid Microshield). The working electrode exposed surface was in the range of 1 cm^2 (accuracy of 1%).

A classic 3-electrode electrochemical cell of 200 mL was used for the electrochemical analysis. The electrochemical cell is provided with quartz window for the photoelectrochemical experiments. A platinum grid was used as counter electrode and a saturated mercury sulphate electrode (MSE, *E* = - 0.64 V/SHE) was used as reference electrode. All experiments were performed in a borate buffer solution (pH = 9 – H_3BO_3 10^{-2} mol/L, Na_2BO_4 3 10^{-2} mol/L) at room temperature. Borate buffer solution was chosen since the oxide film formed on Ni base alloy is poorly soluble in this media, and it was found to be appropriate for the study of the native passive film. Moreover, the presence of Boron in the electrolyte was chosen in order to approach the primary water chemistry which contains boron and lithium. The electrolyte pH at room temperature is slightly alkaline as the simulated primary media. Electrochemical measurements were carried out with a potentiostat/galvanostat (Ref 600) from Gamry Instruments. The passive films were formed at room temperature during 15 hours of immersion at the corrosion potential (E_{corr}) before electrochemical measurements.

Impedance measurements were also performed at corrosion potential during oxidation of the samples at high temperature and high pressure. The high oxidation temperature was maintained for 1000 hours in a static autoclave containing PWR simulated solution with H_2 concentration of at most 35 cm^3/kg (1000 mg/kg of B (H_3BO_3); 2 mg/kg of Li (LiOH)) at 325°C and 130 bars. In the autoclave, the electrochemical measurements were performed using the alloy as a working electrode, a platinum wire as a pseudo-reference and a stainless-steel wire as a counter electrode.

After the film formation, photoelectrochemical measurements were performed using a Xenon arc lamp (Xenon lamp 150W CERMAX) as light source with wavelength varying between 200 and 400 nm. The light beam, collimated by an optical lens, is split and the wavelength is fixed using a digital monochromator. The monochromator position was controlled by a stepping motor with a scan rate of 1 nm/3 s. One of the split-beam is used as a reference and irradiates a calibrated silicon photodiode for flux measurement, and a current-to-voltage converter delivers a voltage signal proportional to the short circuit current of the photodiode. The second split-beam irradiates the electrochemical cell through the quartz window. The quantum yield measurement was then calculated following the Equation .

$$\eta(\lambda) = E\left(\frac{t}{r}\right)\left(\frac{S_{ref}}{S_{Sample}}\right)T\%\left(\frac{I_c(\lambda)}{P_{ref}(\lambda)}\right) \qquad \textit{Equation 1}$$

where η is the quantum yield, λ the wavelength (nm), *E* the energy (eV), *T%* the transmission due to the presence of a protective filter in front of the diode, S_{ref} and S_{sample} are the reference and sample illuminated surface respectively, I_c is the photocurrent (A), P_{ref} is the measured light power (W) and *t/r* a correction factor relative to the transmission *t* and reflection *r* of the beam splitter. The photocurrent was determined from the global measured current after deduction of the corrosion current. The corrosion current was recorded, during the same experiment, just before the illumination of the sample.

Surface state morphology of the samples was characterized by Scanning Electron Microscopy (SEM) (ZEISS Ultra 55).

The oxide film composition was investigated by X-ray Photoelectron Spectroscopy (XPS). Ni2p, Cr2p, Fe2p, O1s and C1s spectra were recorded by an Omicron Argus XPS, equipped with a monochromatic AlK_{α} radiation source (hν = 1486.6 eV). The emission of photoelectrons from the sample was analyzed at a takeoff angle of 90° under ultra-high vacuum conditions (≤ 10^{-10} Torr). Measurements were carried out with a 100 eV pass energy for the survey scan and 20 eV pass energy for the high resolution spectra. The element peak intensities were corrected by Scofield factors [17]. The peak areas were determined after the subtraction of the background using the Shirley method [18]. The spectra were fitted using Casa XPS v.2.3.15 software (Casa Software Ltd., U.K.) and applying a Gaussian/Lorentzian ratio G/L equal to 70/30.

The thickness of oxide film formed on Alloy 690 at high temperature was estimated by Nuclear Reaction Analysis (NRA) using the following reaction $^{16}O + D \leftrightarrow {}^{17}O + H^{+}$. The proton was generated by a 857 KeV incident ^{16}O-beam and was detected at an angle θ = 150°. A 13 µm thick Mylar film prevented back-scattered deuterons from swamping the detector.

3. Results

3.1. Electrochemical behavior of the oxide film formed at room temperature

3.1.1. Current-potential curves

Figure 2 shows the current-potential curves of the Alloy 690 after 15 hours of immersion in the borate buffer solution (pH 9.0). 15 hours of immersion was considered as the required time for passive layer formation and stabilization, from which a pseudo steady state was obtained.

The corrosion potential of the alloy with both surface states, MP and AR, was about -0.55 V/MSE. The passive region extended to about -0.1 V/MSE for the MP tube and to 0 V/MSE for the AR tube. Afterwards the activation peak, a second passive region barely extended over 200 mV with a higher current density was observed. Then, the beginning of the transpassive domain is evidenced by the rise of the current density at 0.4 V/MSE. The second passivation plateau was better evidenced when current-potential curves were performed in steady-state condition (data not presented in this paper). This second passivation plateau is generally attributed to the formation of an oxide film containing mainly Ni and Fe. It can be noted that the activation peak occurred at more anodic potential, with a significant current increase for the AR sample. At potentials greater than 0.4 V/MSE, the increase of current density is related to the oxygen evolution reaction on the material.

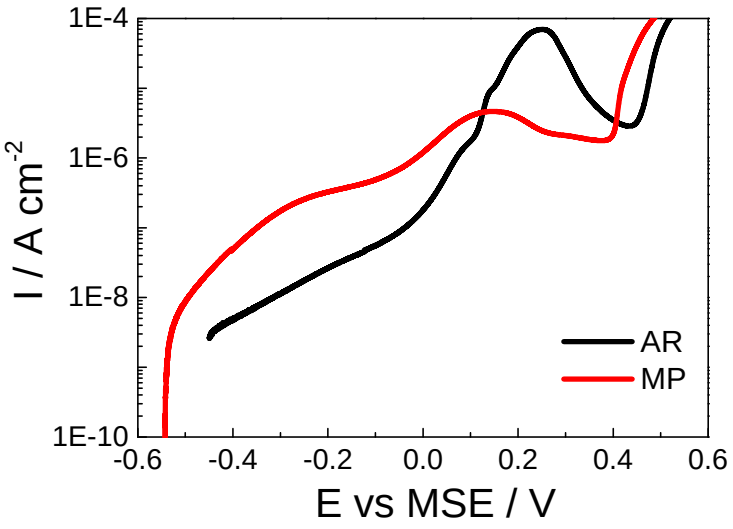

Figure 2: Potentiodynamic polarization curves of the Alloy 690 after 15h immersion at the corrosion potential in borate buffer solution (pH 9.0) at ambient temperature, (v= 0.1 mV/s) for the AR and MP samples

The main difference between both samples is the current density of the first passivation plateau. The AR sample shows a lower passive current density in comparison with the MP sample. A difference in the oxide film composition or thickness may be the origin of this disparity. Moreover, the chromium oxidation occurred at lower potential for the MP sample. The second passivation plateau highlighted similar current density between both materials, but it occurred on a slightly wider potential range on the MP in comparison with the AR.

In order to understand the differences shown on the anodic behaviour, the electrochemical interface of both alloys is investigated by electrochemical impedance spectroscopy after an initial immersion of 15h at the corrosion potential.

3.1.2. Electrochemical impedance spectroscopy

At the corrosion potential (E_{corr}), the global current is equal to zero and the impedance is the sum of the cathodic and anodic contributions operating simultaneously at the electrode surface. In order to determine if one of these contributions dominates, EIS measurements near the corrosion potential (*i.e.* at E_{corr} + 50 mV and E_{corr} - 50 mV) are performed (Figure 3).

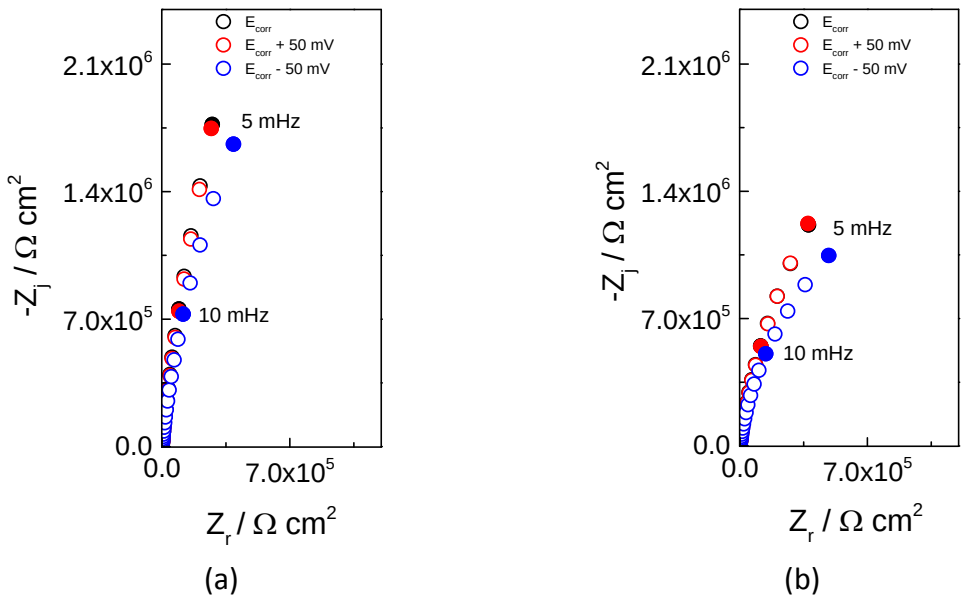

Figure 3: Nyquist diagrams for the AR Alloy 690 (a) and the MP Alloy 690 (b) after 15 h of immersion at E_{corr} in borate buffer solution (pH 9.0) at ambient temperature, measurements at E_{corr}-50 mV, E_{corr} and E_{corr}+50 mV

The impedance diagrams in a Nyquist representation depicted a capacitive behavior showing a slight bending at low frequency, suggesting that the system is tending to a resistance at very low frequency. For both surface states, it was observed that the capacitive loop diameter decreases for a cathodic polarization (E_{corr} - *50 mV*), while the diagrams at corrosion and anodic potentials overlap quite perfectly. This suggests that the impedance measured at corrosion potential is governed by the anodic contribution of the impedance, which is ascribed to the oxidation of the alloy and dissolution of the passive film.

Figure 4 allows to compare the impedance diagrams of both samples, measured after 15 hours of immersion at the corrosion potential. The Nyquist diagrams (Figure 4.a) show the beginning of a capacitive loop as previously described. However, the low-frequency limit decreases significantly for MP alloy thus corresponding to a capacitive loop with a smaller diameter. The Bode diagrams highlight the presence of one time constant at low frequency domain. However, the electrolyte resistance may mask some relevant information on the phase evolution in the high frequency domain. For an easier analysis of the impedance data, the impedance diagrams corrected from the electrolyte resistance are presented in Figure 4.c and Figure 4.d.

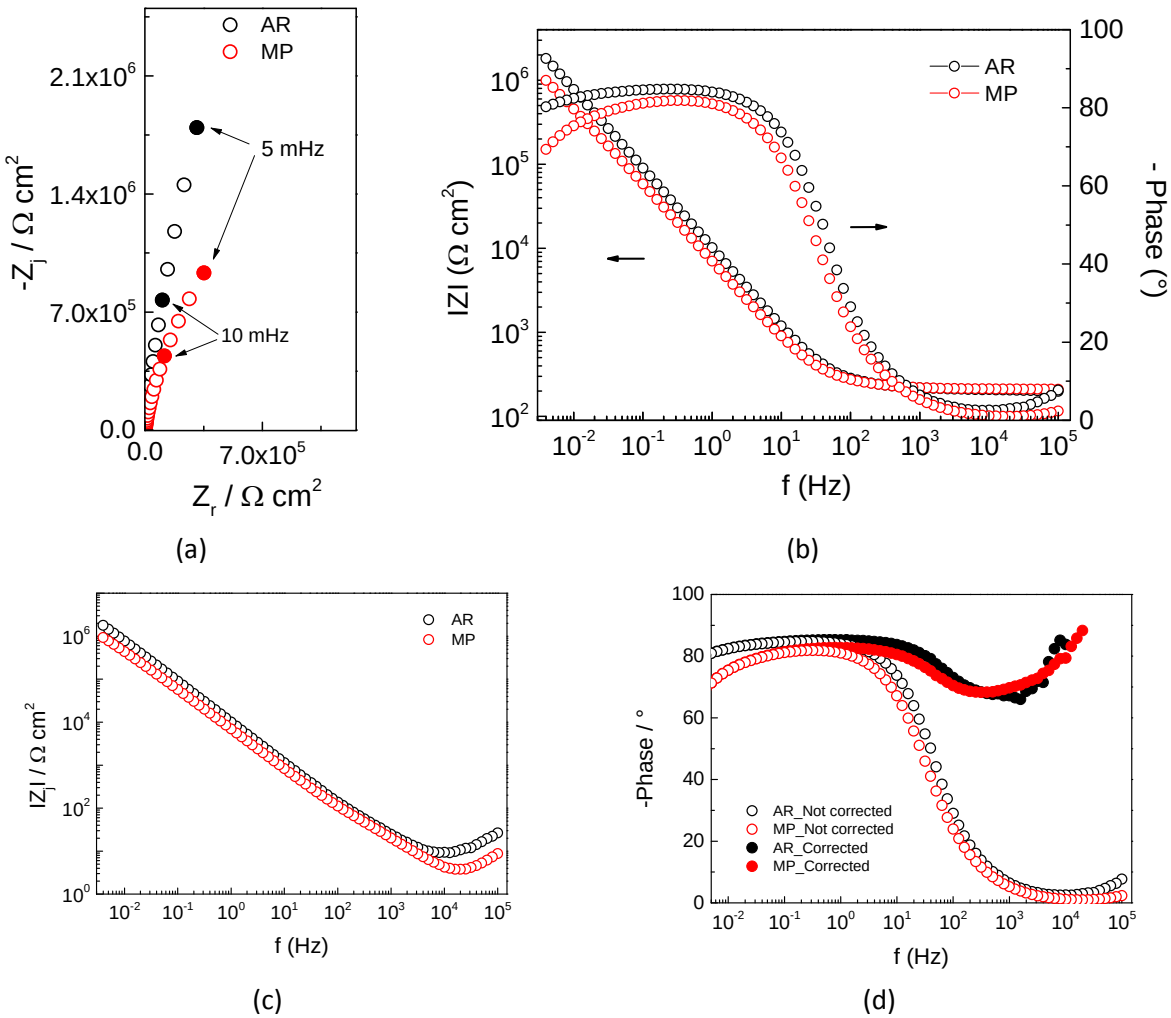

Figure 4: (a) Nyquist, (b) Bode, (c) imaginary part of the impedance part vs. frequency and (d) phase vs. frequency (with and without the correction of R_e) for the Alloy 690 after 15 h of immersion at the corrosion potential in borate buffer solution (pH 9.0) at ambient temperature

The impedance measurements are analyzed with the equivalent electrical circuit presented in Figure 5.a. The circuit represents the oxide film impedance (Z_{film}), which is described by the power-law model (see below), in series with the double layer capacitance, which is described by a constant phase element (CPE_{dl}), both elements being in parallel with the faradaic impedance of the system. For this system and at the corrosion potential, the faradaic impedance is dominated by the anodic branch associated with the film oxidation and the oxide film dissolution and is described by a single charge transfer resistance (R_{tc}). Even though the experimental impedance diagrams are in fact describing the beginning of a semi-circle, the adjusted spectra highlight diagrams in the form of flattened semi-circles, thus justifying the use of a CPE and a specific film impedance to account for the interfacial capacitance.

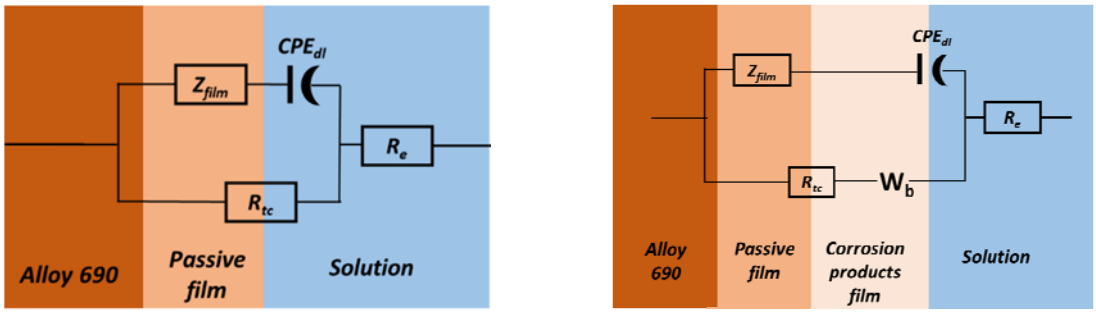

(a) (b)

Figure 5: (a) Equivalent electrical circuit used to analyze impedance measurements of Alloy 690 after 15 h of immersion in borate buffer solution (pH 9.0) at ambient temperature and (b) Equivalent electrical circuit used to analyze impedance measurements of Alloy 690 after 1000 h of oxidation in PWR simulated primary water at 325 °C

The representation of the imaginary part of the impedance *vs.* the frequency in a bi-logarithmic scale (Figure 4.c) shows two linear domains with a slope lower than 1 between (*i*) 10^{-3} and 10 Hz and (*ii*) 40 and 2000 Hz. These two domains are ascribed to two different contributions, both showing a CPE behavior. The correction from the electrolyte resistance is then applied to the experimental data for plotting the phase angle as a function of the frequency (Figure 4.d) [19] . The corrected phase spectra highlights two linear parts over the two same frequency domains previously described on Figure 4.c. A deviation was observed in the high frequency domain, starting from 10^4 Hz, which is ascribed to the geometric effect of the working electrode inducing a significant frequency dispersion that depends, among other, on the electrode size [20].

Because of the non-ideal behavior of the electrochemical system, a constant phase element (CPE) is commonly used to describe the capacitive behavior of the interface, and is expressed as:

$$Z_{CPE} = \frac{1}{Q\ (j\ \omega)^{\alpha}} \qquad \textit{Equation 2}$$

Q and *α,* the CPE parameters, independent of the frequency and *ω*=2πf.

The CPE behavior arises from the dispersion of time constants which are distributed either along the electrode surface (2D distribution) or in the direction normal to the electrode surface (3D distribution). A surface distribution can be generated by surface heterogeneity at the electrode surface such as grain boundaries, crystallographic orientation or a non-uniform distribution of current and potential at the interface due to the electrode geometry. A normal distribution can be expected in systems such as oxide films, in which the distribution of conductivity in the oxide film may vary over a few orders of magnitude, thus resulting in a CPE behavior [21].

Interestingly, the CPE parameters can be readily estimated using a graphical method presented by Orazem et *al.* [22]. α corresponds to the absolute value of the slope of the curve presented in Figure 6.a, that is:

$$\alpha = \left| \frac{d \log |Z_j(f)|}{d \log f} \right| \qquad \textit{Equation 3}$$

and *Q* is calculated from α using the following expression

$$Q = -\frac{1}{Z_j(f)(2\pi f)^{\alpha}} \sin\left(\frac{\alpha\,\pi}{2}\right) \qquad \textit{Equation 4}$$

As shown in Figure 6.a, two linear parts are observed on the curves suggesting the coexistence of two-time constants corresponding to two CPE in series. In the low frequency range corresponding to 10^{-2} to 10 Hz, the CPE is attributed to the double layer capacitance, while the CPE corresponding to the oxide film is highlighted in the high frequency domain.

A normal distribution of time constants linked to the variation of the film resistivity through the oxide film can be well described by the power law model:

$$\frac{\rho}{\rho_\delta} = \left(\frac{\rho_\delta}{\rho_0} + \left(1 - \frac{\rho_\delta}{\rho_0}\right)\xi^{\gamma}\right)^{-1} \qquad \textit{Equation 5}$$

where ρ_0 and ρ_δ are the resistivities at the interface Alloy/oxide and oxide/solution boundaries respectively, and ξ is the dimensionless position within the oxide layer, $\xi = \frac{x}{\delta}$, δ the oxide film thickness, γ is the power law constant linked to the CPE parameter α through $\gamma = \frac{1}{1-\alpha}$.

Using this description of the interface, it is thus possible to access the intrinsic oxide film capacitance and thickness. Assuming that the dielectric constant is uniform within the oxide layer, the impedance of the oxide film is expressed by Equation 6.

$$Z_{film} = g \int_0^1 \frac{\delta\, {\rho_\delta}^{1/\gamma}}{({\rho_0}^{-1} + j\, 2\, \pi\, f\, \varepsilon\, \varepsilon_0)^{(\gamma-1)/\gamma}} \qquad \textit{Equation 6}$$

where g is an expression evaluated numerically [23]:

$$g = 1 + 2.88\, \gamma^{-2.375} \qquad \textit{Equation 7}$$

Additionally, the impedance data presented in Figure 4 can be used in order to determine the oxide film capacitance and thickness, using the complex capacitance representation. Figure 6 shows the complex capacitance plots, obtained from the complex capacitance calculated with Equation 8.

$$C(\omega) = \frac{1}{j\,(Z\,(\omega) - R_e)} \qquad \textit{Equation 8}$$

In the high frequencies, the capacitance tends towards C_∞ and is attributed to the capacitance of the dielectric component of the oxide film. Hence, the oxide film thickness can be estimated using Equation 9.

$$C_{ox} = \frac{\varepsilon\varepsilon_0}{\delta} \qquad \textit{Equation 9}$$

where ε_0 is the permittivity of vacuum (ε_0 = 8.85 10^{-14} F cm^{-1}), ε is the dielectric constant of the oxide film taken equal to 15.6 [24] [25].

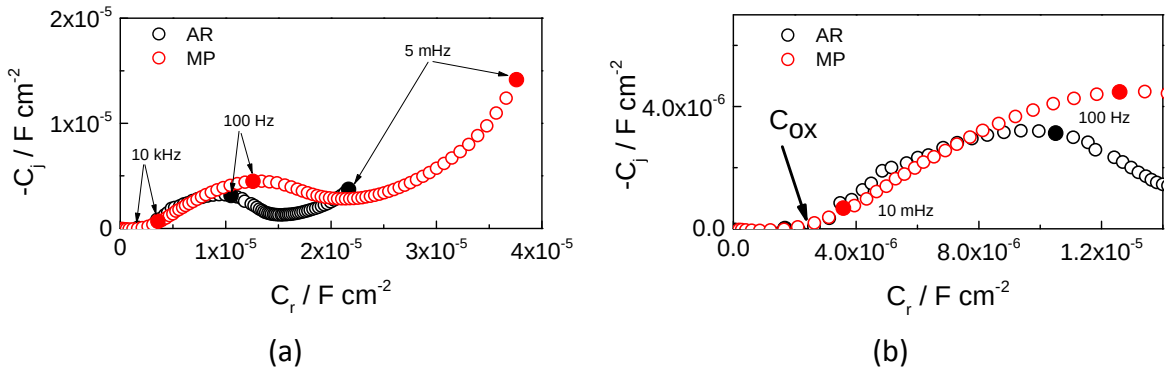

Figure 6: (a) Complex capacitance diagram calculated from the impedance measurements presented in Figure 4 after 15 h of immersion in borate buffer solution (pH 9.0) and (b) determination of the oxide capacitance

The calculated values of both CPE parameters, α and Q, and the oxide capacitance are presented in *Table 2*. The error in the determination of the different parameters was about 5-10%. The oxide film thickness is about 5 to 6 nm which is commonly encountered in the case of passive films on these materials. Independently of the initial surface state, the oxide film formed on Alloy 690 after 15 h of immersion exhibit the same film capacitance and thickness. Following the development of Brug et al. [26] (Equation 10), the double layer capacitance is estimated to be between 10 and 30 µF cm^{-2}, which corresponds to the values commonly encountered in the literature for the double layer capacitance.

$$C_{Brug} = Q^{1/\alpha} R_e^{(1-\alpha)/\alpha} \qquad \textit{Equation 10}$$

Table 2: Parameters determined graphically from the impedance measurements

Alloy 690	Re (Ω cm^2)	CPE_{dl}		C_{dl} (F cm^{-2})	CPE_{film}		C_{ox} (F cm^{-2})	δ (nm)
		α	Q (Ω^{-1} cm^{-2} s$^{\alpha}$)		α	Q (Ω^{-1} cm^{-2} s$^{\alpha}$)		
AR	208	0.94	1.75 10^{-5}	12.2 10^{-6}	0.78	4.39 10^{-5}	2.3 10^{-6}	5.9
MP	212	0.90	2.73 10^{-5}	15.4 10^{-6}	0.74	7.01 10^{-5}	2.4 10^{-6}	5.7

Using the calculated parameters and Equation 5 the distribution of the resistivity within the oxide layer was calculated. At the Alloy/oxide interface (ξ=0), the oxide resistivity is equal to ρ_0. This resistivity decreases along the oxide film thickness and at the oxide/solution interface (ξ=1), the oxide resistivity is equal to ρ_δ. The shape of the resistivity distribution within the oxide film was similar for both samples and show a similar value for the resistivity at both interfaces.

Impedance spectra were then fitted using the electrical equivalent circuit in Figure 5.a with a home-made software. Figure 7 shows the simulated spectra. It can be noted that there is a good agreement between the experimental data and the adjusted graphs. The low frequency domain can thus be obtained by simulating the impedance diagrams for frequency that are not attainable experimentally with the parameters determined from the fitting procedure.

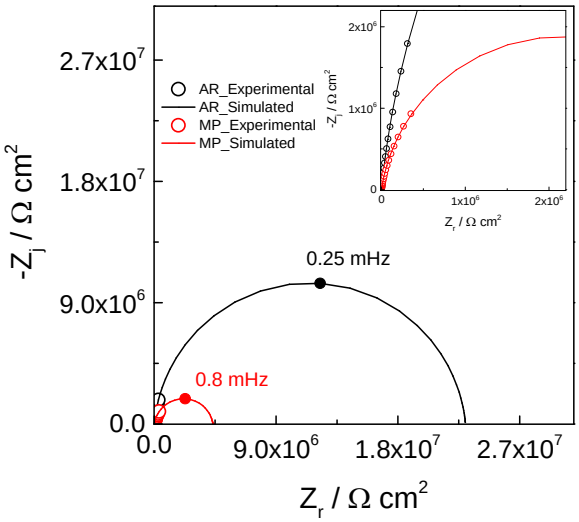

Figure 7: Simulated impedance spectra after 15 h of immersion in borate buffer solution (pH 9.0) at ambient temperature using the electrical equivalent circuit presented in Figure 5.a

The extrapolation at low frequency leads to the determination of R_{tc}, which is linked with the alloy corrosion rate. The values of R_{tc} was equal to 4.3 10^6 Ω.cm^2 for the oxide film formed on the MP alloy and was about 5 times higher for the AR sample (2.3 10^7 Ω.cm^2). Even though the passive film formed on both samples of Alloy 690 has the same oxide capacitance and thickness, their corrosion behavior is different. The comparison of R_{tc} for both alloys suggesting the AR alloy undergoes a smaller corrosion rate in comparison with the MP alloy.

In order to understand the origin of this disparity, the oxide film composition is investigated in the following parts with quantum yield measurements and XPS analysis.

3.2. Oxide film characterization

3.2.1. Photoelectrochemical measurements

Quantum yield measurements were performed on both samples in order to determine and analyze the composition of oxide films formed after 15 h of immersion at the corrosion potential in a borate buffer solution. It is worth noting that the photocurrent measured was negative (data not shown) which is ascribed to p-type semi-conductive properties of the oxide film formed on the AR and MP materials.

The quantum yield measurements enable to determine the composition of passive films by extracting the gap energy. However, it is generally described as more accurate to determine the band gaps using the linear transformation with the following mathematical transformation [27] [28].

$$i_{ph}\, h\nu = A\,(h\nu - E_g)^n \qquad \textit{Equation 11a}$$

where i_{ph} is the photocurrent assumed to be proportional to the optical absorption coefficient, $h\nu$ is the photon energy, A a constant and E_g is the gap energy. The exponent n is related to the type of transition between the valence band and the conduction band. For amorphous films, such as passive films, the transitions are generally indirect, and the value of n commonly used is ½. In this work, the quantum yield formula is used instead of i_{ph}.

Figure 8 shows the different contributions after the mathematical transformation *(η x hv)*$^{1/2}$ *vs hv*. The optical band gaps are extracted graphically from the linear parts of the graph at the intersection with the x-axis. *Table 3* gathers the different band gaps extracted at low energy, between 3.0 and 5.0 eV.

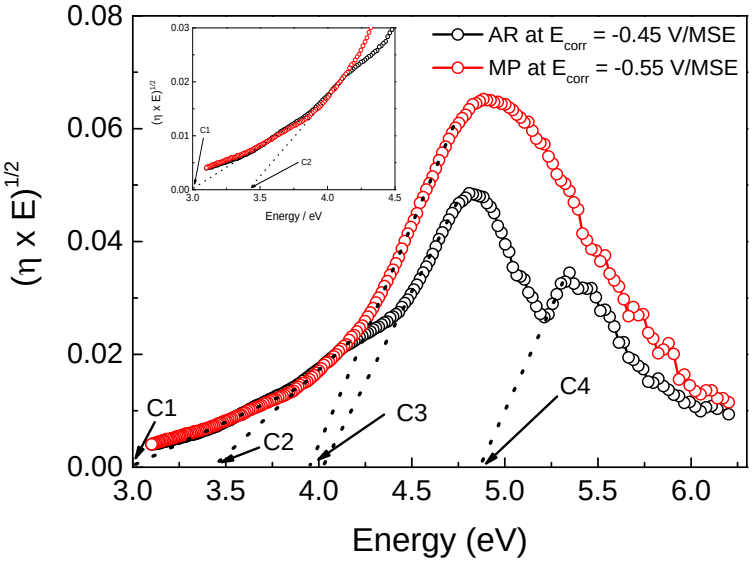

Figure 8: Determination of band gaps from quantum yield measurements using the transformation presented in Equation 11a

Table 3: Band gaps extracted from Figure 8

Alloy 690	C1 (eV)	C2 (eV)	C3 (eV)	C4 (eV)
AR	2.9	3.3	4.0	4.8
MP	2.9	3.4	3.9	-

At low energy, three common contributions between 2.9 to 4.0 eV are observed on both samples of the Alloy 690. A fourth contribution at *ca* 4.8 eV was only observed for the AR alloy.

The gap energy determined at 4.0 eV for AR and 3.9 eV for MP, is attributed to NiO. NiO is a p-type semiconductor material presenting a band gap situated between 3.7 and 3.9 eV [29] [30] [31]. In some other works, it is reported that the band gap of NiO can be extended till 4.0 eV [32] [33].

The value of 3.5 eV is commonly attributed to the Cr_2O_3 [34]. However, and depending on the experimental conditions and parameters, the band gap of Cr_2O_3 can be located between 3.0 and 3.5 eV [35] [36] [37]. The contribution C2 exhibited values between 3.0 and 3.5 eV, and accordingly, C2 is attributed to Cr_2O_3.

The contribution C1 is smaller in term of intensity than C2 and C3. Moreover, it overlaps with the tailing of the curve resulting in a larger uncertainty in the determination of the band gap energy. However, C1 showed values around 2.9 eV. This band gap can correspond to a minor contribution of $Ni(OH)_2$, hydrated Cr(III) oxide or a mixed Ni-Cr hydroxide. Indeed, for this contribution, the literature gives very varied attributions. Hermet *et al.* [38] attributed to the *β*-$Ni(OH)_2$ a band gap equal to 2.9 eV. Similarly, H.J. Jang *et al.* [39] analysed the photoelectrochemical response of passive film formed on pure Ni in a pH 8.5 borate solution and they observed a band gap of $Ni(OH)_2$ of 3.05 ± 0.1 eV. It is also reported in the literature that the band gap of hydrated Cr(III) oxide is close to the value obtained for $Ni(OH)_2$. Sunseri *et al.* [34] and Di Quarto et al [37] attributed a band gap of 2.90 to 2.95 eV to CrOOH. J.S.Kim

et al. [40] measured on pure Cr in a 8.5 pH borate solution, two gap energies at 2.75 and 3.0 eV, which were attributed to $Cr(OH)_3$ and CrOOH, respectively. Nevertheless, some other works attributed a band gap of 2.5 eV to the $Cr(OH)_3$ compound [34] [37] [41].

Thus, the photoelectrochemical response of the passive film formed on the MP and the AR Alloy 690, mainly originates from NiO with minor contributions of Cr_2O_3 and Ni-Cr hydroxides. These results are in agreement with some previous works on Ni-based alloys at room temperature [15] [42].

The AR alloy exhibited a fourth photoelectrochemical contribution leading to a band gap of about 4.8 eV, which can be ascribed to the presence of the mixed spinel $Ni(Fe,Cr)_2O_4$. Marchetti *et al.* [43] attributed to the mixed spinel phase $Ni_{(1-x)}Fe_xCr_2O_4$ a band gap between 4.1 and 4.5 eV. They measured a band gap of 4.1 eV on the passive film formed on Ni-30Cr alloys, which was attributed to the $NiCr_2O_4$ compound. On the Alloy 690, they measured a band gap ranged between 4.4 and 4.5 eV which was attributed to the mixed spinel $Ni_{(1-x)}Fe_xCr_2O_4$. These authors suggested that the substitution of Ni by Fe in the oxide film can induce such a change for the band gap, leading to a shift of the energy towards higher values. Recent works confirm the attribution of the band gap in high energies (4.3 – 4.8 eV) to the mixed spinel phase $Ni_{(1-x)}Fe_xCr_2O_4$ [44] [45].

It is well known that the oxide film formed on Ni base alloy has a duplex structure with an internal part rich in Cr and an outer part mainly composed with Ni and Fe crystallites [4] [6] [46]. The internal part of the oxide film to which is attributed the protective effect against corrosion is known to be composed of a compact continuous layer of Cr_2O_3 covered by a mixed spinel type nickel chromite $Ni(Fe,Cr)_2O_4$.

The Alloy 690 once manufactured is in fact thermally annealed between 950 and 1100°C. Many studies indicated the presence of nickel chromite oxide within the oxide film formed during this thermal oxidation and its coexistence with Cr_2O_3 and NiO on Ni-Cr Alloys [47] [48]. As a consequence, one can admit that the passive film initially formed on the AR alloy is composed of Ni and Cr oxides with the presence of mixed spinel $Ni(Fe,Cr)_2O_4$. This native passive layer is removed during the mechanically polishing.

Such a chemical composition of the passive film of the AR sample is well supported by the quantum yield measurements. The presence of this additional oxide on the AR alloy can also explain the difference observed for the charge transfer resistance. In order to confirm these results, XPS analyses were performed.

3.2.2. XPS analysis

XPS analysis were performed after 15 h of immersion in borate buffer solution in order to identify the chemical composition of the oxide layers formed on both samples. Only the chromium, nickel and oxygen profiles were analyzed. The iron is not one of the major compounds of the oxide film formed with these conditions and was difficult to detect. Figure 9 shows the XPS profiles of the passive film formed on both samples of Alloy 690.

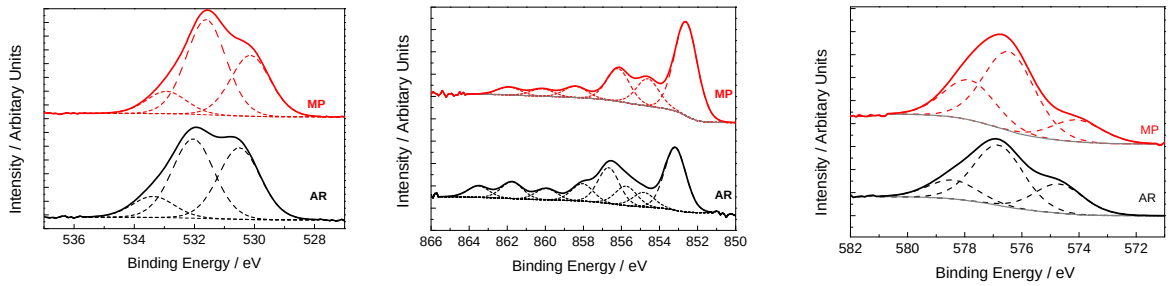

(a) **(b)** **(c)**

Figure 9: XPS spectra and deconvolution curves of (a) O1s, (b) Ni-2p3/2 and (c) Cr-2p3/2 of the passive film formed on Alloy 690 after 15 h of immersion in a borate buffer solution (pH 9.0)

Table 4 gathers the experimental binding energies (BE) determined from the XPS spectra deconvolution and their attribution to the oxide and hydroxide species on the basis of the BE in the literature.

Table 4: Binding energies determined from XPS spectra deconvolution and their attribution to the different compounds of the O 1s, Ni 2p3/2 and Cr 2p3/2

		BE (eV)			
		Position	Ref.	MP	AR
O 1s	Oxide	530.0 ± 0.4	[49] [50] [51]	530.1	530.5
	Hydroxide	531.5 ± 0.5	[49] [51] [52] [53]	531.6	532.0
	Adsorbed H_2O	533.2 ± 0.2	[49] [51]	532.9	533.3
Ni 2p3/2	Ni(0)	852.9 ± 0.3	[49] [51] [54]	852.5	853.1
	Ni^{2+} (NiO)	854,4 ± 0.4	[49] [54]	854.6	854.4
	Ni^{2+} ($Ni(OH)_2$)	856.4 ± 0.4	[55] [56]	856.2	856.6
	Ni^{2+} ($Ni(Cr,Fe)O_4$)	855.8 ± 0.2	[57] [51]	-	855.8
Cr 2p3/2	Cr(0)	573.9 ± 0.4	[56] [51]	574.0	574.5
	Cr^{3+} (Cr_2O_3)	576.0 ± 0.5	[50] [57]	576.4	576.8
	Cr^{3+} ($Cr(OH)_3$)	577.0 ± 0.5	[56] [58] [59]	577.8	578.4

XPS spectra performed on the passive films formed on both samples show that the films are mainly composed of Cr and Ni oxides and hydroxides, which is consistent with results reported in other works [15] [60]. The presence of the $Ni(Fe,Cr)_2O_4$ mixed spinel compound is only observed on the AR alloy, which is consistent with the quantum yield measurements performed in this work.

3.3. Oxide film behavior at high temperature

3.3.1 Electrochemical measurements

Figure 10 presents the impedance spectra on the MP and the AR Alloy 690 samples obtained at 325°C in PWR simulated primary water at the corrosion potential during 1000 h of oxidation. The Nyquist diagrams describe flattened capacitive loop. The loop diameter significantly increases with time between 24 and 1000 h of oxidation time. Conversely to the impedance measurements performed at room temperature, the MP and the AR alloys show the same electrochemical response. This suggests that the passive film formed on both samples have the same physical properties and/or chemical composition.

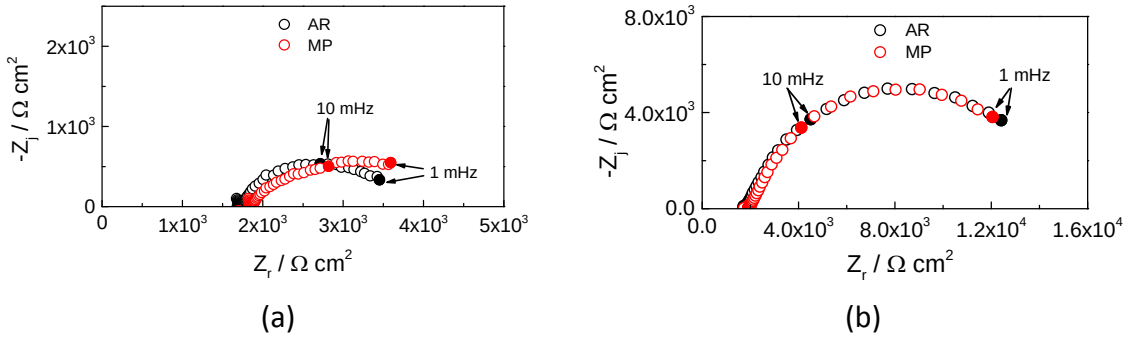

Figure 10: Nyquist diagrams of the MP and AR Alloy 690 after (a) 24 h and (b) 1000 h of immersion at E_{corr} in a simulated primary water of PWR at 325°C and 130 bars

Moreover, at high frequency domain, the impedance spectra highlight a linear part along a slight section which ends up describing a loop at low frequencies. The slope of the linear section corresponds to a 45° angle thus suggesting the presence of a diffusion process. Assuming as previously that the global impedance is governed by the anodic branch of the faradaic reaction, the impedance measurements were analyzed with the equivalent electrical circuit presented in Figure 5.b. Conversely to the behavior at room temperature, the impedance spectra at high temperature show a diffusional contribution that can be related to the diffusion of ions through the corrosion products.

Figure 11 presents the experimental and fitted impedance spectra performed with the equivalent circuit presented in Figure 5.b after 1000 h of oxidation at high temperature and pressure, and Table 5 gathers the different parameters obtained from the fitting procedure. The α parameter of CPE_{dl} is about 0.8 while it is only 0.45 for CPE_{film}. Such a low value for α suggests that the film formed at high temperature is porous, in agreement with the de Levie works [61].

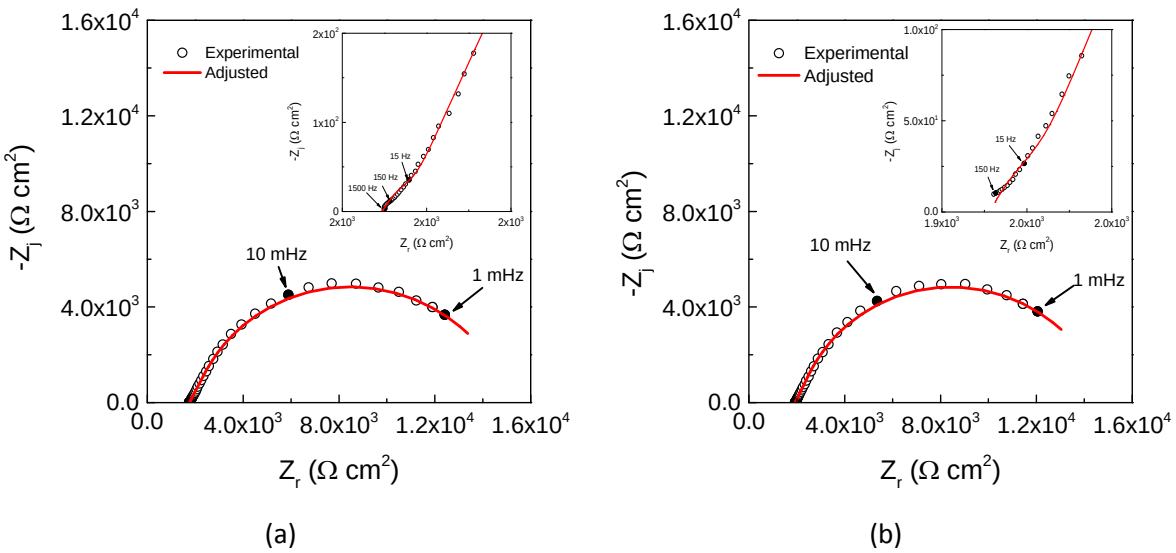

Figure 11: Adjusted impedance spectra of (a) AR and (b) MP samples after 1000 h of oxidation in simulated primary water at high temperature using the equivalent electrical circuit presented in Figure 5.b

Table 5: Parameters extracted from the fitting of the impedance spectra at 1000 h immersion time

Alloy 690	Re (Ω cm²)	CPE $_{dl}$		Z_{film}			R_{tc} (Ω cm²)	R_D (Ω cm²)
		α	Q (Ω^{-1} cm^{-2} s^{α})	α	ρ_0 (Ω cm)	ρ_δ (Ω cm)		
AR	1750	0.82	1.8 10^{-3}	0.45	26 10^{8}	8.2 10^{3}	25	1.3 10^{4}
MP	1924	0.86	2.5 10^{-3}	0.45	2.0 10^{8}	3.3 10^{3}	56	1.3 10^{4}

Both samples show similar properties in terms of oxide resistivity, diffusion and charge transfer resistance. The latter strongly decreases at high temperature due to the thermal activation of the (electro)chemical reactions.

The oxide films formed at high temperature were characterized again at room temperature and the behavior initially depicted was re-observed. We could hence estimate the charge transfer resistances using the equivalent circuit in Figure 5.a which were around 1.3 10^7 and 6 10^6 Ω.cm² for the AR and MP samples, respectively. These values are very close to the ones initially estimated at room temperature.

Moreover, the complex capacitance representation was used to determine the oxide film thickness after 1000 h oxidation at high temperature. Values around 2-4 nm were obtained for both samples, slightly smaller than the thickness estimated at room temperature. This difference is ascribed to the elimination of hydroxides during the high temperature oxidation process.

One can conclude that the internal layer at the Alloy/oxide interface initially formed at room temperature, is preserved after a 1000 hours oxidation at 325°C in autoclave conditions.

3.3.2. Oxide film thickness

Nuclear Reaction Analyses (NRA) were performed on both oxidized samples in order to determine the oxygen concentration within the oxide film and the oxide layer thickness (Figure 12).

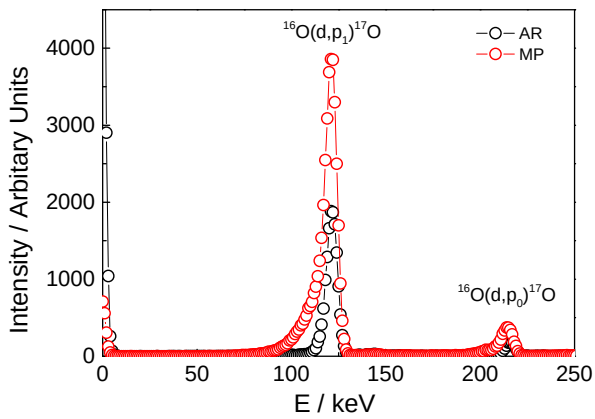

Figure 12: NRA spectra obtained with incident energy of Deuterium with 857 keV for both oxidized samples

The oxygen amount within the passive film formed on the MP alloy was higher than in the passive film formed on the AR alloy. Assuming that the oxide film is compact with a uniform thickness and formed by a single type of oxide, an equivalent thickness can be calculated from the NRA analysis as:

$$\delta_{Ox} = \frac{A}{\rho\, N\, y}\, Q_{NRA} \qquad \textit{Equation 1b}$$

where δ_{ox} is the thickness of the oxide layer, A is the molar mass of the oxide (g mol^{-1}), ρ is the oxide density (g cm^{-3}), N is Avogadro number, y is the oxygen stoichiometry in the oxide film and Q_{NRA} is the quantity of oxygen measured by NRA.

Assuming that the oxide layer formed on both samples is mostly composed of inner layer of Cr_2O_3 and an external layer of a mixed Cr-Fe-Ni spinel, the oxide layer formed on the AR sample was estimated to have a thickness of about 58 nm, and about 3 times thicker on the MP sample. These thicknesses are in agreement with the observations reported in the literature [46].

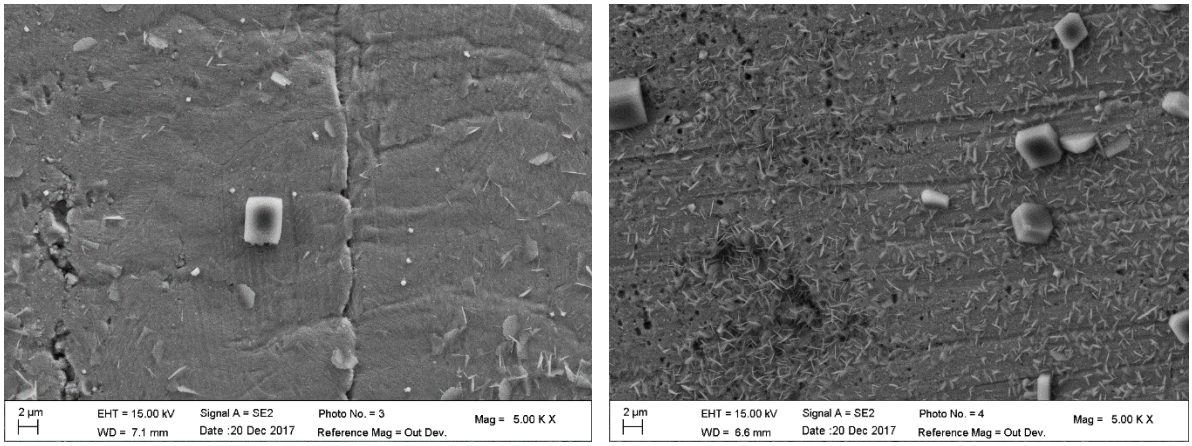

(a) (b)

Figure 13: SEM observations of the oxide films formed on the AR (a) and the MP (b) Alloy 690 after 1000 h of oxidation in PWR simulated primary water

Moreover, SEM observations were performed on both samples (Figure 13). Conversely to the experiments performed at low temperature and short immersion time, the presence of oxide particles can be observed. The size of the oxide crystallites exhibits similar shape on both alloys, but there are more of them on the MP alloy. Hang et al. [55] [62] studied the effect of surface state on the oxide growth on Alloy 690 but for short duration of oxidation at high temperature and high pressure. They concluded that the oxide films have the same composition for the oxide layer and only the film thickness depended on the surface finishing and the surface roughness. Different authors mentioned this effect of the surface finishing and suggest that polishing promotes oxide growth leading to thicker oxide layer on alloys and stainless steel [62] [63] [64] [65].

The thicknesses estimated from NRA measurements (50-150 nm) are ascribed to the total oxide film including mainly the corrosion product layer, while the thicknesses determined by EIS (2-4 nm) is related to the internal layer at the Alloy/oxide interface, only.

4. Discussion

On the basis of the XPS analysis and quantum yield measurements, a model of the passive film formed on the Alloy 690 at room temperature is proposed in Figure 14 to account for all the results presented in this work.

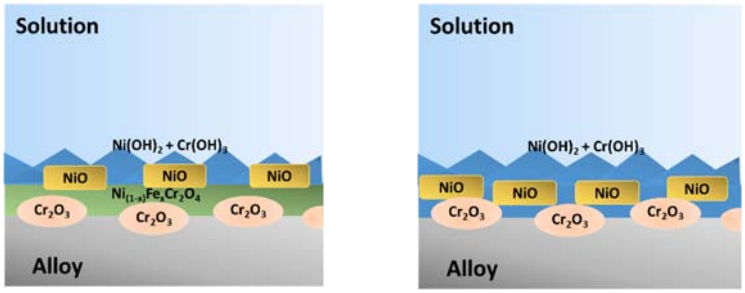

(a) **(b)**

Figure 14: Model of the passive film formed on the AR (a) and MP (b) Alloy 690 in a borate buffer solution (pH 9.0) at ambient temperature

The film formed on the Alloy 690 is composed of an inner oxide film enriched in Cr. For the AR alloy, this layer is composed of Cr_2O_3 and a mixed Ni-Cr spinel type $Ni_{(1-x)}Fe_xCr_2O_4$, while it only contains Cr_2O_3 on the MP alloy. This internal part is overlayed by an external one mainly composed of Ni oxide and Ni,Cr hydroxide. Our model is developed on the basis of the experimental results presented in this paper and on the basis of literature depth profiling of passive film formed on Ni base alloy. AES depth profiling studies [13] [66] [67] have demonstrated that the passive film formed on Ni base alloys is formed with internal Cr oxide covered with Ni and Fe oxides. Similar results on the composition of passive film formed at ambient temperature on the Alloy 690 mention the presence of Ni oxide as a top layer coexisting with hydrated phase of Ni and Cr, over a Cr rich layer [15] [55].

It was shown that EIS is an efficient tool for analyzing the passivation behavior of the Alloy/oxide interface. At room temperature, the initially formed passive film was found to be 4-6 nm thick. The charge transfer resistance, R_{tc}, around 10^7 Ω cm^2, is strongly related to the initial surface coverage with Cr containing species. Due to the thermal activation, the interface becomes active with R_{tc} values as low as 20-50 Ω cm^2. At 325°C, electrochemical corrosion takes place at the alloy surface not covered by Cr oxide, with the release of metal cations. In autoclave conditions, no temperature gradient exists at the interface and the transport of cations including Cr ions by diffusion is efficient. As a consequence, there is no Cr enrichment of the inner passive layer which becomes a few thinner (2-4 nm) probably due to the disappearance of hydroxides. The precipitation of the corrosion products gives rise to a porous, a few tens of nm thick layer acting as a diffusion barrier for ions. It is thus concluded that oxidation process in autoclave at 325°C does not modify the passivating properties of the inner layer as demonstrated by the same R_{tc} values measured before and after the high temperature oxidation. Additionally, the presence of mixed Ni-Cr-Fe spinel within the passive film (AR alloy) was found to be beneficial for the protection of the alloy against corrosion.

Concerning the effect of illumination, a p-type semiconducting response was mainly obtained for the passive films formed on the Alloy 690 at room temperature. This p-type semiconducting response is attributed to the nickel oxide NiO, in agreement with the results of Park *et al.* [68] on pure Ni in pH 8.5 buffer borate solution. Such a film exhibited p-type semiconducting properties and they have shown that an increase in the solution temperature leads to an increase in the concentration of cation vacancies.

On the other hand, the internal sub-layer of the oxide film formed on the Alloy 690 at high temperature is composed of Cr_2O_3 and mixed Ni-Fe-Cr spinel through which the transport of mainly Ni and Fe species contributing to the oxide growth occurs through a solid state process [3]. It is believed that the internal

layer is formed by an anionic diffusion process along a short-circuit network such as grain boundaries [2]. However, Fe and Ni diffusion through the internal part proceeds to the edification of the outer part of the oxide film and involves cationic vacancies within the alloy. The experiments presented in this work give evidence for the already presence of $Ni(Cr,Fe)O_4$ within the passive film on the AR alloy resulting from the manufacturing process of the material. Increasing the oxidation temperature involve so the preferential consumption of Cr and nucleation of Cr_2O_3 [5], the insertion of Ni and Fe and their diffusion through the Cr_2O_3 layer leading to the formation of $Ni_{(1-x)}FexCr_2O_4$. Moreover, it is reported that surface dislocations of the material contribute to an increase in the anionic and cationic diffusion coefficients during high temperature oxidation and oxide film growth [2]. Although the internal part of the passive layer formed on the MP alloy at room temperature is only formed with Cr oxide, oxidation at high temperature promote the growth of $Ni_{(1-x)}Fe_xCr_2O_4$ phase which is enhanced by the surface defects resulting from the polishing. However, the characterization of the oxide film performed at room temperature after high temperature oxidation gave identical parameters to those obtained for the initial native film. Thus, from EIS experiments, it is shown that the oxidation at 325°C in autoclave is not accompanied by Cr enrichment of the inner oxide layer, whatever the presence or not of the spinel phase. This means that the Cr ions diffusion is the key parameter controlling Cr deposition at the Alloy/oxide interface, which is a too fast process at 325°C in static thermal conditions.

Exposure to high temperature brings the passive film formed on the MP and the AR alloy to the same composition with a significantly larger thickness than at low temperature, rising mainly from the corrosion products layer. The oxide layer formed on the MP alloy is 3 times thicker than on the AR alloy. This was directly related to the surface treatment and defect density, in agreement with the work of Cissé et al. [63], who suggested that the grinding of the sample promotes the formation of recrystallized areas. The thinner this recrystallized layer, the faster the diffusion of species forming the oxide film happens and the thicker the passive film.

Conclusions

The electrochemical behavior and chemical composition of the passive film formed on two different surface finishing of the Alloy 690 at room temperature were investigated in a pH = 9.0 borate buffer solution. On the basis of the XPS analysis, it was shown that the passive film formed on the MP material contains Ni and Cr oxides and hydroxides. The presence of mixed spinel type $Ni_{(1-x)}Fe_xCr_2O_4$ was only evidenced on the AR Alloy. This finding was confirmed by quantum yield measurements. At room temperature, the presence of mixed spinel type $Ni(Cr,Fe)O_4$ on the AR Alloy leads to higher charge transfer resistance measured for the MP sample, thus corresponding to a better corrosion resistance. For comparison with what found at ambient temperature, the AR and MP samples were characterized at high temperature in a static autoclave simulating the PWR primary water circuit. It was shown that the interface becomes electrochemically active with the temperature rising. At a surface temperature of 325°C, diffusion of metal cations was found to be a fast process hampering the Cr enrichment of the Alloy/oxide interface. EIS and NRA analyses allowed to characterize the surface film actually composed of two layers: (i) an inner one, a few nm thick, very similar to the passive layer initially formed at ambient temperature; (ii) an outer one, much thicker (a few tens of nm) but less dense, due to the precipitation of the corrosion products electrochemically produced and acting as a diffusion barrier for the released metal cations. The results presented in this paper are consistent with the fact that it is demonstrated that the very thin and dense Cr containing layer at the Alloy/oxide interface is maintained the same during and after high temperature oxidation in static thermal

autoclave condition, without permanent modification of the passivation behavior after such a high temperature oxidation sequence.

References

[1] L. Guinard, O. Kerrec, D. Noel, S. Gardey, et F. Coulet, « Influence of initial surface condition on the release of nickel alloys in the primary circuit of PWRs », *Nucl. Energy*, vol. 36, n° 1, p. 19–27, 1997.

[2] H. Lefaix-Jeuland, L. Marchetti, S. Perrin, M. Pijolat, M. Sennour, et R. Molins, « Oxidation kinetics and mechanisms of Ni-base alloys in pressurised water reactor primary conditions: Influence of subsurface defects », *Corros. Sci.*, vol. 53, n° 12, p. 3914–3922, déc. 2011.

[3] L. Marchetti, S. Perrin, F. Jambon, et M. Pijolat, « Corrosion of nickel-base alloys in primary medium of pressurized water reactors: New insights on the oxide growth mechanisms and kinetic modelling », *Corros. Sci.*, vol. 102, n° Supplement C, p. 24–35, janv. 2016.

[4] F. Carrette, M. C. Lafont, G. Chatainier, L. Guinard, et B. Pieraggi, « Analysis and TEM examination of corrosion scales grown on Alloy 690 exposed to pressurized water at 325 °C », *Surf. Interface Anal.*, vol. 34, n° 1, p. 135–138, août 2002.

[5] M. Sennour, L. Marchetti, S. Perrin, R. Molins, M. Pijolat, et O. Raquet, « Characterization of the oxide films formed at the furface of Ni-Base alloys in pressurized water reactors primary coolant bytransmission electron microscopy », *Mater. Sci. Forum*, vol. 595–598, p. 539–547, 2008.

[6] M. Sennour, L. Marchetti, F. Martin, S. Perrin, R. Molins, et M. Pijolat, « A detailed TEM and SEM study of Ni-base alloys oxide scales formed in primary conditions of pressurized water reactor », *J. Nucl. Mater.*, vol. 402, n° 2, p. 147–156, juill. 2010.

[7] L. Marchetti, S. Perrin, O. Raquet, et M. Pijolat, « Corrosion Mechanisms of Ni-Base Alloys in Pressurized Water Reactor Primary Conditions », *Mater. Sci. Forum*, vol. 595–598, p. 529–537, 2008.

[8] F. Delabrouille, L. Legras, F. Vaillant, P. Scott, B. Viguier, et E. Andrieu, « Effect of the chromium content and strain on the corrosion of nickel based alloys in primary water of pressurized water reactors », présenté à 12th International conference on Environmental Degradation of Materials in Nuclear Power System - Water Reactors, 2005.

[9] D. H. Hur, J. H. Han, U. C. Lee, et Y. S. Park, « Microchemistry of Ti-Carbonitrides and Their Role in the Early Stage of Pit Initiation of Alloy 600 », *CORROSION*, vol. 62, n° 7, p. 591–597, juill. 2006.

[10] F. Carrette, « Relâchement des produits de corrosion des tubes en alliage 690 de générateur de vapeur du circuit primaire des réacteurs à eau pressurisée », Thèse, Toulouse, INPT, 2002.

[11] L. Guinard, O. Kerrec, S. Gardey, et D. Noel, « Investigations for reducing the release of steam generator materials: experiments and modeling », présenté à JAIF international conference on water chemistry in nuclear power plants, Japan, 1998.

[12] T. Jabs, P. Borthen, et H.-H. Strehblow, « X-Ray Photoelectron Spectroscopic Examinations of Electrochemically Formed Passive Layers on Ni-Cr Alloys », *J. Electrochem. Soc.*, vol. 144, n° 4, p. 1231–1243, avr. 1997.

[13] S. Boudin *et al.*, « Analytical and electrochemical study of passive films formed on nickel—chromium alloys: Influence of the chromium bulk concentration », *Surf. Interface Anal.*, vol. 22, n° 1–12, p. 462–466, juill. 1994.

[14] J. Steffen et S. Hofmann, « Oxidation of NiCr and NiCrFe alloys at room temperature », *Surf. Interface Anal.*, vol. 11, n° 12, p. 617–626, sept. 1988.

[15] H. J. Jang et H. S. Kwon, « Effects of Film Formation Conditions on the Chemical Composition and the Semiconducting Properties of the Passive Film on Alloy 690 », *Corros. Sci. Technol.*, vol. 5, n° 4, p. 141–148, 2006.

[16] A. Machet, « Etude des premiers stades d'oxydation d'alliages inoxydables dans l'eau à haute température », Thèse, Université Paris 6, 2004.

[17] J. H. Scofield, « Hartree-Slater subshell photoionization cross-sections at 1254 and 1487 eV », *J. Electron Spectrosc. Relat. Phenom.*, vol. 8, n° 2, p. 129–137, janv. 1976.
[18] D. A. Shirley, « High-Resolution X-Ray Photoemission Spectrum of the Valence Bands of Gold », *Phys. Rev. B*, vol. 5, n° 12, p. 4709–4714, juin 1972.
[19] B. Hirschorn, M. Orazem, B. Tribollet, V. Vivier, I. Frateur, et M. Musiani, « Constant-Phase-Element Behavior Caused by Resistivity Distributions in Films II. Applications », *J. Electrochem. Soc.*, vol. 157, p. C452–C457, janv. 2010.
[20] I. Frateur, V. M.-W. Huang, M. E. Orazem, N. Pébère, B. Tribollet, et V. Vivier, « Local electrochemical impedance spectroscopy: Considerations about the cell geometry », *Electrochimica Acta*, vol. 53, n° 25, p. 7386–7395, oct. 2008.
[21] V. M.-W. Huang, V. Vivier, M. E. Orazem, N. Pébère, et B. Tribollet, « The Apparent Constant-Phase-Element Behavior of an Ideally Polarized Blocking Electrode A Global and Local Impedance Analysis », *J. Electrochem. Soc.*, vol. 154, n° 2, p. C81–C88, févr. 2007.
[22] M. E. Orazem, N. Pébère, et B. Tribollet, « Enhanced Graphical Representation of Electrochemical Impedance Data », *J. Electrochem. Soc.*, vol. 153, n° 4, p. B129–B136, avr. 2006.
[23] B. Hirschorn, M. E. Orazem, B. Tribollet, V. Vivier, I. Frateur, et M. Musiani, « Constant-Phase-Element Behavior Caused by Resistivity Distributions in Films I. Theory », *J. Electrochem. Soc.*, vol. 157, n° 12, p. C452–C457, déc. 2010.
[24] J. Huang, X. Wu, et E.-H. Han, « Electrochemical properties and growth mechanism of passive films on Alloy 690 in high-temperature alkaline environments », *Corros. Sci.*, vol. 52, n° 10, p. 3444–3452, oct. 2010.
[25] N. S. McIntyre, D. G. Zetaruk, et D. Owen, « XPS study of the initial growth of oxide films on Inconel 600 alloy », *Appl. Surf. Sci.*, vol. 2, n° 1, p. 55–73, nov. 1978.
[26] G. J. Brug, A. L. G. van den Eeden, M. Sluyters-Rehbach, et J. H. Sluyters, « The analysis of electrode impedances complicated by the presence of a constant phase element », *J. Electroanal. Chem. Interfacial Electrochem.*, vol. 176, n° 1, p. 275–295, sept. 1984.
[27] U. Stimming, « Photoelectrochemical studies of passive films », *Electrochimica Acta*, vol. 31, n° 4, p. 415–429, avr. 1986.
[28] M. A. Butler, « Photoelectrolysis and physical properties of the semiconducting electrode WO2 », *J. Appl. Phys.*, vol. 48, n° 5, p. 1914–1920, mai 1977.
[29] F. Di Quarto, S. Piazza, et C. Sunseri, « Photoelectrochemistry in Corrosion Studies: Achievements and Perspectives », *Mater. Sci. Forum - MATER SCI FORUM*, vol. 192–194, p. 633–648, janv. 1995.
[30] G. Dagan, W.-M. Shen, et M. Tomkiewicz, « Passivation of Permalloy Thin Films II . In Situ Characterization of the Oxide Layer by Photoelectrochemical and Impedance Measurements », *J. Electrochem. Soc.*, vol. 139, n° 7, p. 1855–1861, juill. 1992.
[31] M. P. Dare-Edwards, J. B. Goodenough, A. Hamnett, et N. D. Nicholson, « Photoelectrochemistry of nickel(II) oxide », *J. Chem. Soc. Faraday Trans. 2 Mol. Chem. Phys.*, vol. 77, n° 4, p. 643–661, 1981.
[32] R. J. Powell et W. E. Spicer, « Optical Properties of NiO and CoO », *Phys. Rev. B*, vol. 2, n° 6, p. 2182–2193, sept. 1970.
[33] R. Newman et R. M. Chrenko, « Optical Properties of Nickel Oxide », *Phys. Rev.*, vol. 114, n° 6, p. 1507–1513, juin 1959.
[34] C. Sunseri, S. Piazza, et F. D. Quarto, « Photocurrent Spectroscopic Investigations of Passive Films on Chromium », *J. Electrochem. Soc.*, vol. 137, n° 8, p. 2411–2417, août 1990.
[35] S. Henry, J. Mougin, Y. Wouters, J.-P. Petit, et A. Galerie, « Characterization of Chromia Scales Grown on Pure Chromium in Different Oxidizing Atmospheres », *Mater. High Temp.*, vol. 17, n° 2, p. 231–234, mai 2000.
[36] A. Galerie, S. Henry, Y. Wouters, M. Mermoux, J.-P. Petit, et L. Antoni, « Mechanisms of chromia scale failure during the course of 15–18Cr ferritic stainless steel oxidation in water vapour », *Mater. High Temp.*, vol. 22, n° 1–2, p. 105–112, janv. 2005.

[37] F. Di Quarto, S. Piazza, et C. Sunseri, « A photocurrent spectroscopic investigation of passive films on chromium », *Corros. Sci.*, vol. 31, p. 721–726, janv. 1990.
[38] P. Hermet *et al.*, « Dielectric, magnetic, and phonon properties of nickel hydroxide », *Phys. Rev. B*, vol. 84, nº 23, p. 235211, déc. 2011.
[39] H. Jang, C. Park, et H. Kwon, « Photoelectrochemical analysis on the passive film formed on Ni in pH 8.5 buffer solution », *Electrochimica Acta*, vol. 50, nº 16, p. 3503–3508, mai 2005.
[40] J. Kim, E. Cho, et H. Kwon, « Photo-electrochemical analysis of passive film formed on Cr in pH 8.5 buffer solution », *Electrochimica Acta*, vol. 47, nº 3, p. 415–421, oct. 2001.
[41] H. Tsuchiya, S. Fujimoto, O. Chihara, et T. Shibata, « Semiconductive behavior of passive films formed on pure Cr and Fe–Cr alloys in sulfuric acid solution », *Electrochimica Acta*, vol. 47, nº 27, p. 4357–4366, oct. 2002.
[42] H. Jang et H. Kwon, « Photoelectrochemical analysis of passive films formed on Ni and its alloys and its application to their corrosion behaviors », *J. Solid State Electrochem.*, vol. 19, nº 12, p. 3427–3438, déc. 2015.
[43] L. Marchetti, S. Perrin, Y. Wouters, F. Martin, et M. Pijolat, « Photoelectrochemical study of nickel base alloys oxide films formed at high temperature and high pressure water », *Electrochimica Acta*, vol. 55, nº 19, p. 5384–5392, juill. 2010.
[44] L. Latu-Romain, Y. Madi, S. Mathieu, F. Robaut, J.-P. Petit, et Y. Wouters, « Advanced STEM/EDX investigation on an oxide scale thermally grown on a high-chromium iron–nickel alloy under very low oxygen partial pressure », *Corros. Sci.*, vol. 101, p. 193–200, déc. 2015.
[45] F. Mechehoud, N. E. Benaioun, N. E. Hakiki, A. Khelil, L. Simon, et J. L. Bubendorff, « Thermally oxidized Inconel 600 and 690 nickel-based alloys characterizations by combination of global photoelectrochemistry and local near-field microscopy techniques (STM, STS, AFM, SKPFM) », *Appl. Surf. Sci.*, vol. 433, p. 66–75, mars 2018.
[46] A. Machet, A. Galtayries, P. Marcus, P. Combrade, P. Jolivet, et P. Scott, « XPS study of oxides formed on nickel-base alloys in high-temperature and high-pressure water », *Surf. Interface Anal.*, vol. 34, nº 1, p. 197–200, août 2002.
[47] C. Greskovich, « Kinetics of NiCr2O4 Formation and Diffusion of Cr3+ Ions in NiO », *J. Am. Ceram. Soc.*, vol. 53, nº 9, p. 498–502, 1970.
[48] H. Davies et W. W. Smeltzer, « Oxygen and Metal Activities of the Chromium-Nickel-Oxygen System Between 900° and 1100°C », *J. Electrochem. Soc.*, vol. 121, nº 4, p. 543–549, avr. 1974.
[49] M. C. Biesinger, B. P. Payne, L. W. M. Lau, A. Gerson, et R. S. C. Smart, « X-ray photoelectron spectroscopic chemical state quantification of mixed nickel metal, oxide and hydroxide systems », *Surf. Interface Anal.*, vol. 41, nº 4, p. 324–332, avr. 2009.
[50] M. C. Biesinger, C. Brown, J. R. Mycroft, R. D. Davidson, et N. S. McIntyre, « X-ray photoelectron spectroscopy studies of chromium compounds », *Surf. Interface Anal.*, vol. 36, nº 12, p. 1550–1563, déc. 2004.
[51] M. C. Biesinger, B. P. Payne, A. P. Grosvenor, L. W. M. Lau, A. R. Gerson, et R. S. C. Smart, « Resolving surface chemical states in XPS analysis of first row transition metals, oxides and hydroxides: Cr, Mn, Fe, Co and Ni », *Appl. Surf. Sci.*, vol. 257, nº 7, p. 2717–2730, janv. 2011.
[52] A. N. Mansour et C. A. Melendres, « Characterization of α-Ni(OH)2 by XPS », *Surf. Sci. Spectra*, vol. 3, nº 3, p. 255–262, juill. 1994.
[53] N. S. McIntyre et M. G. Cook, « X-ray photoelectron studies on some oxides and hydroxides of cobalt, nickel, and copper », *Anal. Chem.*, vol. 47, nº 13, p. 2208–2213, nov. 1975.
[54] A. P. Grosvenor, M. C. Biesinger, R. S. C. Smart, et N. S. McIntyre, « New interpretations of XPS spectra of nickel metal and oxides », *Surf. Sci.*, vol. 600, nº 9, p. 1771–1779, mai 2006.
[55] F. Huang, J. Q. Wang, E. H. Han, et W. Ke, « Short-time Oxidation of Alloy 690 in High-temperature and High-pressure Steam and Water », *J. Mater. Sci. Technol.*, vol. 28, nº 6, p. 562–568, juin 2012.
[56] A. Mazenc, « Caractérisation par ToF-SIMS des couches de passivation des tubes de générateurs de vapeur en Alliage 690 pour l'industrie nucléaire : apport à la compréhension des mécanismes », Thèse, Université Paris 6, 2013.

[57] L. Marchetti, F. Miserque, S. Perrin, et M. Pijolat, « XPS study of Ni-base alloys oxide films formed in primary conditions of pressurized water reactor », *Surf. Interface Anal.*, vol. 47, n° 5, p. 632–642, mai 2015.
[58] E. Ünveren, E. Kemnitz, S. Hutton, A. Lippitz, et W. E. S. Unger, « Analysis of highly resolved x-ray photoelectron Cr 2p spectra obtained with a Cr2O3 powder sample prepared with adhesive tape », *Surf. Interface Anal.*, vol. 36, n° 1, p. 92–95, janv. 2004.
[59] I. Grohmann, E. Kemnitz, A. Lippitz, et W. E. S. Unger, « Curve fitting of Cr 2p photoelectron spectra of Cr2O3 and CrF3 », *Surf. Interface Anal.*, vol. 23, n° 13, p. 887–891, déc. 1995.
[60] L. Marchetti-Sillans, « Corrosion généralisée des alliages à base nickel en milieu aqueux à haute température : Apport à la compréhension des mécanismes », Thèse, Ecole Nationale Supérieure des Mines de Saint-Etienne, 2007.
[61] Sluyters-Rehbach, M., Timmer, B., et Kooyman, D.J., « Paul Delahay, Editor, Advances in Electrochemistry and Electrochemical Engineering, Vol. 6, Electrochemistry, Interscience Publishers, New York (1967) », *J. Electroanal. Chem.*, vol. 22, n° 2, p. 275null, août 1969.
[62] F. Huang, J. Wang, E.-H. Han, et W. Ke, « Microstructural characteristics of the oxide films formed on Alloy 690 TT in pure and primary water at 325°C », *Corros. Sci.*, vol. 76, p. 52–59, nov. 2013.
[63] S. Cissé, L. Laffont, B. Tanguy, M.-C. Lafont, et E. Andrieu, « Effect of surface preparation on the corrosion of austenitic stainless steel 304L in high temperature steam and simulated PWR primary water », *Corros. Sci.*, vol. 56, p. 209–216, mars 2012.
[64] M. Warzee, J. Hennaut, M. Maurice, C. Sonnen, J. Waty, et P. Berge, « Effect of Surface Treatment on the Corrosion of Stainless Steels in High-Temperature Water and Steam », *J. Electrochem. Soc.*, vol. 112, n° 7, p. 670–674, juill. 1965.
[65] Z. Zhang, J. Wang, E.-H. Han, et W. Ke, « Characterization of Different Surface States and Its Effects on the Oxidation Behaviours of Alloy 690TT », *J. Mater. Sci. Technol.*, vol. 28, n° 4, p. 353–361, avr. 2012.
[66] G. Lorang, N. Jallerat, K. V. Quang, et J.-P. Langeron, « AES depth profiling of passive overlayers formed on nickel alloys », *Surf. Interface Anal.*, vol. 16, n° 1–12, p. 325–330, juill. 1990.
[67] J. Steffen et S. Hofmann, « Oxidation of NiCr and NiCrFe alloys at room temperature », *Surf. Interface Anal.*, vol. 11, n° 12, p. 617–626, sept. 1988.
[68] K. Park, S. Ahn, et H. Kwon, « Effects of solution temperature on the kinetic nature of passive film on Ni », *Electrochimica Acta*, vol. 56, n° 3, p. 1662–1669, janv. 2011.